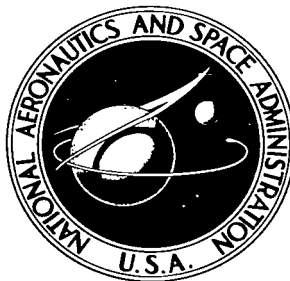


NASA TECHNICAL NOTE



NASA TN D-3106

e. 1

NASA TN D-3106

LOAN COPY: RETURN TO
AFWL (VLL-2)
KIRTLAND AFB, NM

0130051

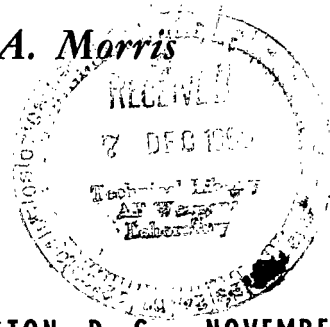


A WIND-TUNNEL INVESTIGATION OF THE EFFECT OF BODY SHAPE ON SONIC-BOOM PRESSURE DISTRIBUTIONS

by Harry W. Carlson, Robert J. Mack, and Odell A. Morris

Langley Research Center

Langley Station, Hampton, Va.



NATIONAL AERONAUTICS AND SPACE ADMINISTRATION - WASHINGTON, D. C. - NOVEMBER 1965



A WIND-TUNNEL INVESTIGATION OF THE EFFECT OF BODY SHAPE
ON SONIC-BOOM PRESSURE DISTRIBUTIONS

By Harry W. Carlson, Robert J. Mack,
and Odell A. Morris

Langley Research Center
Langley Station, Hampton, Va.

NATIONAL AERONAUTICS AND SPACE ADMINISTRATION

For sale by the Clearinghouse for Federal Scientific and Technical Information
Springfield, Virginia 22151 - Price \$2.00

A WIND-TUNNEL INVESTIGATION OF THE EFFECT OF BODY SHAPE
ON SONIC-BOOM PRESSURE DISTRIBUTIONS

By Harry W. Carlson, Robert J. Mack,
and Odell A. Morris
Langley Research Center

SUMMARY

Measurements of sonic-boom pressure distributions at distances of up to 20 body lengths from eight slender bodies of revolution have been made at Mach numbers of 1.26, 1.41, and 2.01. The results show that pressure-signature measurements are in good agreement with near-field theory and that values of maximum-overpressure parameter are often much lower than indicated by far-field theory. The blunt far-field lower-bound body had higher near-field overpressures than other shapes, but also had the lowest measured pressure-signature impulse.

INTRODUCTION

In recent years considerable research effort has been devoted to the problem of minimizing sonic-boom overpressures. Optimization studies have been based on the methods of references 1 and 2 for relating flow-field pressures to wing-body geometry. In reference 3, the dependence of far-field overpressures for complete airplanes on an equivalent-body area distribution including both volume and lift contributions was discussed, a series of effective-area-distribution shapes was studied, and a body shape corresponding to an approximate lower bound was found. The more rigorous solution of reference 4 showed that an absolute minimum far-field overpressure for a body of revolution of given length and maximum cross-sectional area is found when the area, except in the immediate vicinity of the nose, varies as the square root of the distance from the nose. According to theory, the blunt shape in reference 4 yields not only the minimum far-field overpressure but also produces the minimum pressure-signature impulse at all distances. Later studies reported in reference 5 have indicated the possibilities of other boom-minimization concepts based on the observation that in some cases, such as for a large supersonic transport configuration in the transonic-acceleration portion of flight, the near field may extend from the airplane to the ground. In such a situation, where the shape of the signature is controlled by the airplane geometry, it may be possible to modify the

signature and reduce overpressures through detailed airplane design. Effective-area-distribution shapes tending to produce this result have a very gradual buildup in area and show some promise for successful application to airplane design.

Since boom-minimization concepts are dependent on the applicability of the methods of reference 1 in estimating the flow characteristics about bodies of revolution, pressure measurements have been made for eight slender bodies of revolution and the results have been compared with theoretical estimates. The investigation was conducted in the Langley 4- by 4-foot supersonic pressure tunnel at Mach numbers of 1.26, 1.41, and 2.01. Pressure measurements were made at distances of up to 40 inches (101.6 cm) from the models, all of which were 2 inches (5.08 cm) in length. Each of the models had a maximum cross-sectional area of 0.04 square inch (0.26 cm²). This maximum area is representative of the nondimensionalized effective area for a supersonic transport configuration in the transonic-acceleration portion of the flight. Models included three cones, a far-field lower-bound shape, a minimum-drag body, a double cone, and two other configurations.

SYMBOLS

Measurements for this investigation were taken in the U.S. Customary System of Units. Equivalent values are indicated herein parenthetically in the International System (SI) in the interest of promoting use of this system in future NASA reports. Details concerning the use of SI, together with physical constants and conversion factors, are given in reference 6.

A	cross-sectional area of model determined by supersonic-area-rule cutting planes having an angle μ with respect to the longitudinal axis
A(t)	nondimensionalized cross-sectional area A/l^2 at nondimensionalized station $t = x/l$
F(τ)	area distribution function, $\frac{1}{2\pi} \int_0^\tau \frac{A''}{\sqrt{\tau-t}} dt$
h	perpendicular distance from model to measuring probe
K _M	Mach number factor, $\frac{\gamma+1}{\sqrt{2}} \frac{M^4}{(M^2-1)^{3/4}}$
K _R	reflection factor
k	constant in body-shape equation
l	model reference length
l _c	cone length
2	

M	Mach number
n	bluntness parameter
p	free-stream static reference pressure
Δp	incremental pressure due to flow field of model
Δp_{\max}	maximum value of Δp
r	radius of model
t	nondimensionalized distance measured along longitudinal axis from model nose, x/l
x	distance measured along longitudinal axis from model nose
ΔX	distance from point on pressure signature to point where pressure-signature curve crosses zero-pressure reference axis
$\beta = \sqrt{M^2 - 1}$	
θ	cone half-angle
γ	ratio of specific heats (1.4 for air)
μ	Mach angle, $\sin^{-1} \frac{1}{M}$
τ	dummy variable of integration measured in same direction and using same units as t
τ_0	value of τ giving largest positive value of the integral $\int_0^{\tau} F(\tau) d\tau$

A prime is used to indicate a first derivative and a double prime is used to indicate a second derivative with respect to distance along the model axis.

MODELS AND APPARATUS

Drawings of the test models and equations for the radius distribution are given in figure 1. Models 1, 2, and 3 are cones having cone half-angles of 3.24° , 6.46° , and 12.75° , respectively. Model 4 has a linear distribution of normal cross-sectional area. Model 5 is based on the lower-bound shape of reference 4. The model as constructed departs from the theoretical shape only in the vicinity of the nose, where the condition $A'(t) = 0$ is not met. Model 6 is one of the shapes found in reference 3 to have relatively good boom characteristics. Model 7 is the von Kármán minimum-drag body of given length and given base diameter. Although it appears to be pointed, this model is blunt,

the derivative dr/dx being infinite at $x = 0$. Model 8 is a double cone. The afterbody for each of the models is a circular cylinder having a cross-sectional area of 0.04 square inch (0.26 cm²). Each model is assumed to have a reference length of 2 inches (5.08 cm).

The investigation was conducted in the Langley 4- by 4-foot supersonic pressure tunnel at Mach numbers of 1.26, 1.41, and 2.01 with a stagnation pressure of 10 psi (69 kN/m²) and a stagnation temperature of 100° F (311° K). A sketch of the wind-tunnel apparatus is shown in figure 2. Both the model and the measuring probes were mounted on a support system which provided for remote-control adjustments of longitudinal and lateral position. The probes were very slender cones (1° cone half-angle), each having four 0.013-inch-diameter (0.033-cm) static pressure orifices leading to a common chamber. Orifices were circumferentially spaced 90° apart and were arranged to lie in a Mach 1.4 cone originating at the model. A more detailed discussion of wind-tunnel sonic-boom test techniques is given in reference 7.

THEORETICAL CONSIDERATIONS

Theoretical determination of the pressure fields about the test models by the method of reference 1 is illustrated in figure 3. The area distribution function $F(\tau)$ which is of paramount importance in the subsequent pressure-signature determination was found by an application of the smooth-body equation:

$$F(\tau) = \frac{1}{2\pi} \int_0^\tau \frac{A''(t)}{\sqrt{\tau-t}} dt \quad (1)$$

The required area development ($A(t)$) was evaluated through employment of supersonic-area-rule concepts, the cross-sectional area at any body station being determined by the frontal projection onto a plane normal to the model axis of the area intercepted by a cutting plane inclined at the Mach angle and passing through the longitudinal axis at the body station. Application of supersonic-area-rule concepts and use of equation (1) constitute a method of analysis particularly suitable to complex airplane configurations, since such a method provides for the proper superposition of the flow contributions from separate airplane elements. Area developments for the bodies were found by use of the supersonic-area-rule wave-drag computer program described in reference 8. Evaluation of the F function as given by equation (1) was performed by a machine computing program described in appendix A of reference 7. The small circular symbols shown for the area-distribution-function parameter in figure 3 are machine program results. A fairing of these data as shown by the solid-line curve was used for subsequent operations. According to the analysis in reference 1, the incremental pressure (Δp) at any point in the

flow field ($x - \beta h, h$) may be determined from this curve for the area-distribution-function parameter by constructing a line having a slope of $\frac{1}{K_m \sqrt{h}}$ through the point $\tau = \frac{x - \beta h}{l}$ and noting its intersection with the curve, the pressure being related to $F(\tau)$ as follows:

$$\frac{\Delta p}{p} = \frac{F(\tau)}{\sqrt{h}} \frac{\gamma}{\sqrt{2}} \frac{M^2}{(M^2 - 1)^{1/4}} \quad (2)$$

In regions of this curve for which multiple values of Δp occur, the original curve is replaced by the straight line segment of slope $\frac{1}{K_m \sqrt{h}}$ which is passed through the curve so that lobe areas balance as illustrated in the figure. This procedure, of course, leads to the formation of the shocks shown in theoretical pressure signatures.

The more rigorous solution of reference 1 for nonsmooth bodies of revolution which employs the Heaviside unit step function and the Stieltjes integral has been found to give a better representation of the flow pattern in the region influenced by the body discontinuity than does the smooth-body solution used herein. However, in the numerical application of the nonsmooth-body method, some difficulty in obtaining a proper solution for blunt bodies such as the lower-bound shape was encountered in the present investigation. In the region of the near singularity of the F function at $\tau = 0$, the entire area under the curve could be approximated only by the employment of extremely small intervals. Use of the numerical method of determining the F function given in reference 7 which provides an integrated area independent of the tabulation for $F(\tau)$ was found to overcome the problem. With the exception of the blunt-nosed bodies, choice of either the smooth or nonsmooth solution has little effect on the pressure signature ahead of the trailing shock and thus would not alter any conclusions referring to maximum overpressure or impulse.

When it is known beforehand that for the conditions under consideration a far-field signature having a simple N-shape will exist, it is possible to make a simplification in the theory. Values of far-field maximum overpressure (Δp_{\max}) may be found from an integration of the area under the function $F(\tau)$ in the following equation:

$$\frac{\Delta p_{\max}}{p} = \frac{K_r \beta^{1/4}}{\left(\frac{h}{l}\right)^{3/4}} \frac{1.19 \gamma}{\sqrt{\gamma + 1}} \sqrt{\int_0^{\tau_0} F(\tau) d\tau} \quad (3)$$

RESULTS AND DISCUSSION

Pressure signatures were measured in the supersonic flow fields of the models at zero angle of attack and the pressure distributions are shown in figure 4. Pressures and

distances are presented in parametric form in accordance with theoretical considerations. When far-field conditions are reached, signatures assume a characteristic N-shape and when plotted in the parametric form remain identical as distance is increased. However, only for the large-half-angle cones (models 2 and 3) is an approach to far-field conditions noted within the allowable tunnel separation distances. Each of the measured signatures is compared with a theoretical near-field signature and, for reference, theoretical far-field signatures are superimposed for several of the models. The rounding of the measured pressure peaks is believed to be due in part to wind-tunnel vibration and boundary-layer effects discussed in reference 7. In general, the measured results and the near-field theory are in very good agreement. It is noted that the agreement is reasonably good even for a body as blunt as the lower-bound shape which violates the assumptions of the linearized theory on which the solution is based.

Data for the series of cone models illustrated in figure 5 are useful in examining the effect of distance and rate of area development cone half-angle on the pressure-signature characteristics. The variation of maximum-overpressure parameter with cone half-angle for measurements taken at 10 body lengths from the models in Mach 1.41 flow is shown in figure 6. Inset sketches show the relative shape and magnitude of the signatures for the three cone models. These data clearly indicate the strong influence of cone half-angle on the characteristics of the signature and on the degree to which far-field conditions are approached. At the smaller cone half-angles, values of the maximum-overpressure parameter are much lower than indicated by far-field theory. It can be observed that a break occurs in the near-field-theory curve at a cone half-angle slightly below 8° and that, for larger half-angles, both near-field theory and experiment show values of maximum-overpressure parameter only slightly below estimates based on the far-field assumption. This break is characteristic for cones and may exist for other bodies with surface discontinuities.

Figure 7 shows the variation of the maximum-overpressure parameter with distance for the 6.46° half-angle cone (model 2). A constant value of the parameter indicates a maximum overpressure (Δp_{\max}) which varies as the inverse of the three-quarter power of the distance. Inset sketches show the pressure signatures corresponding to the test distances of 5, 10, and 20 body lengths. Near-field theory and experimental data closely approach far-field theory at a distance of about 32 body lengths.

The dependence of the overpressure characteristics of the cone series on the combined effects of cone half-angle and distance may be observed in the parametric plot of figure 8. The parameters, which were derived from theoretical considerations, allow the theory to be shown for the most part as a single line. In this figure it is necessary that the nondimensionalizing model dimension be taken as the cone length l_c rather than the arbitrary reference length l . It may be seen that the near-field theory is in good agreement with the measured data. For values of the cone-half-angle—distance parameter

$\frac{h}{l_c} \theta^4$ greater than about 10^5 , the pressure signature would display far-field characteristics with maximum overpressures only slightly lower than those estimated by far-field theory.

An illustration of the variation of near-field maximum-overpressure parameter with Mach number is given in figure 9. Data are shown for the intermediate half-angle cone (model 2) at a distance of 10 body lengths. This figure shows that, as predicted by near-field theory, Mach number has a strong influence on the pressure-signature shape. At Mach numbers of 1.26 and 1.41, signatures display near-field characteristics whereas, at a Mach number of 2.01, far-field conditions have essentially been met.

Figure 10 shows the correlation between measured values and theoretical estimates of signature impulse $\left(\int \frac{\Delta p}{p} d\left(\frac{x}{l}\right)\right)$ for the range of cone half-angles. The theory (for near field and far field) predicts that the impulse is proportional to the inverse of the one-half power of the distance. Thus, a constant value of the parameter $\int \frac{\Delta p}{p} d\left(\frac{x}{l}\right) \left(\frac{h}{l}\right)^{1/2}$ at all distances for a given cone half-angle indicates an impulse decrease, as predicted by theory. Data for all three of the test distances at $M = 1.41$ are in reasonably good agreement with the theoretical estimates. The cone half-angle or the rate of the area development is seen to have a strong influence on the signature impulse, the more gradual area development of the slender cone creating a smaller impulse.

The variation of signature-impulse parameter with Mach number for the intermediate half-angle cone is shown in figure 11. Data for all the distances at each test Mach number are seen to be in reasonable agreement with the theory.

A series of three body shapes with various degrees of nose bluntness is illustrated in figure 12. Model 1, a cone model previously discussed, obviously has a sharp nose shape, but is included in the comparison because it is a member of a family of mathematical shapes expressed by the equation $r = kx^n$. Model 4 ($n = 0.50$) has a linear distribution of cross-sectional area and thus has a somewhat blunt nose. Model 5 ($n = 0.25$) represents the far-field lower-bound shape and has an extremely blunt nose. The area developments shown in this figure have been obtained through use of Mach 1.41 cutting planes. The bluntness parameter n is defined by the equation $r = kx^n$ representing the body shape.

Variation of maximum-overpressure parameter with bluntness parameter is presented in figure 13, and inset sketches show the shape of the signatures measured at a distance of 10 body lengths from each of the three models in the bluntness series in Mach 1.41 flow. Measured values are compared with estimates based on both near-field and far-field theory. It may be noted that, for the far-field lower-bound shape (model 5; $n = 0.25$), near-field theory and far-field theory give identical results. The fact that the measured value of maximum-overpressure parameter for this shape is lower than the

theoretical estimates is believed to be due in large part to wind-tunnel vibration and boundary-layer effects. At larger values of the bluntness parameter, considerably reduced values of maximum-overpressure parameter which are much lower than estimates based on far-field assumptions but which are in good agreement with the near-field theory are noted. A minimum value of maximum-overpressure parameter would appear to occur at $n \approx 0.75$.

Variation of signature-impulse parameter with bluntness parameter for the same three models is shown in figure 14. Because near-field theory and far-field theory give identical values of impulse parameter, only one theory curve is required. It is of interest to note that the blunt lower-bound shape, for which the maximum near-field overpressures were larger than for the other two shapes had the lowest measured values of impulse as indicated by theory. This result serves to confirm the theoretical indications that the blunt lower-bound shape would produce a far-field overpressure lower than the far-field overpressure for any other shape. However, signatures for the lower-bound shape display far-field characteristics very close to the body, whereas for other shapes the far-field conditions are reached only at very large distances. In addition, it should be noted that the lower-bound shape has an extremely high wave drag.

The overall correlation of theoretical and experimental overpressure and impulse parameters may be observed in figures 15 and 16. It has been noted that the largest discrepancies from the perfect agreement line in the overpressure plot occur for the blunt bodies (models 4, 5, and 7) and for the larger half-angle cones with sharp signature peaks (models 2 and 3). In spite of these discrepancies, however, the overall correlation is reasonably good.

CONCLUDING REMARKS

A wind-tunnel investigation of the supersonic flow fields about eight slender bodies of revolution has been conducted at Mach numbers of 1.26, 1.41, and 2.01. The investigation has shown that pressure-signature measurements taken at distances of up to 20 body lengths from the models are in good agreement with near-field theory and that values of maximum-overpressure parameter are often much lower than estimates based on far-field assumptions. This result lends support to previous analytical studies which indicated that, for supersonic transport configurations in the transonic-acceleration portion of flight, airplane design could be modified to produce significant reduction in maximum sonic-boom overpressure.

Even for very blunt-nosed bodies for which application of a theory based on slender-body concepts would appear to be questionable, near-field theory and experiment were found to be in reasonably good agreement. The blunt far-field lower-bound body had

higher near-field overpressures than other shapes, but also had the lowest measured pressure-signature impulse.

Langley Research Center,
National Aeronautics and Space Administration,
Langley Station, Hampton, Va., September 9, 1965.

REFERENCES

1. Whitham, G. B.: The Flow Pattern of a Supersonic Projectile. Commun. Pure and Appl. Math., vol. V, no. 3, Aug. 1952, pp. 301-348.
2. Walkden, F.: The Shock Pattern of a Wing-Body Combination, Far From the Flight Path. Aeron. Quart., vol. IX, pt. 2, May 1958, pp. 164-194.
3. Carlson, Harry W.: The Lower Bound of Attainable Sonic-Boom Overpressure and Design Methods of Approaching This Limit. NASA TN D-1494, 1962.
4. Jones, L. B.: Lower Bounds for Sonic Bangs. J. R.A.S. (Tech. Notes), vol. 65, no. 606, June 1961, pp. 433-436.
5. McLean, F. Edward: Some Nonasymptotic Effects on the Sonic Boom of Large Airplanes. NASA TN D-2877, 1965.
6. Mechtly, E. A.: The International System of Units - Physical Constants and Conversion Factors. NASA SP-7012, 1964.
7. Carlson, Harry W.: Correlation of Sonic-Boom Theory with Wind-Tunnel and Flight Measurements. NASA TR R-213, 1964.
8. Harris, Roy V., Jr.: An Analysis and Correlation of Aircraft Wave Drag. NASA TM X-947, 1964.

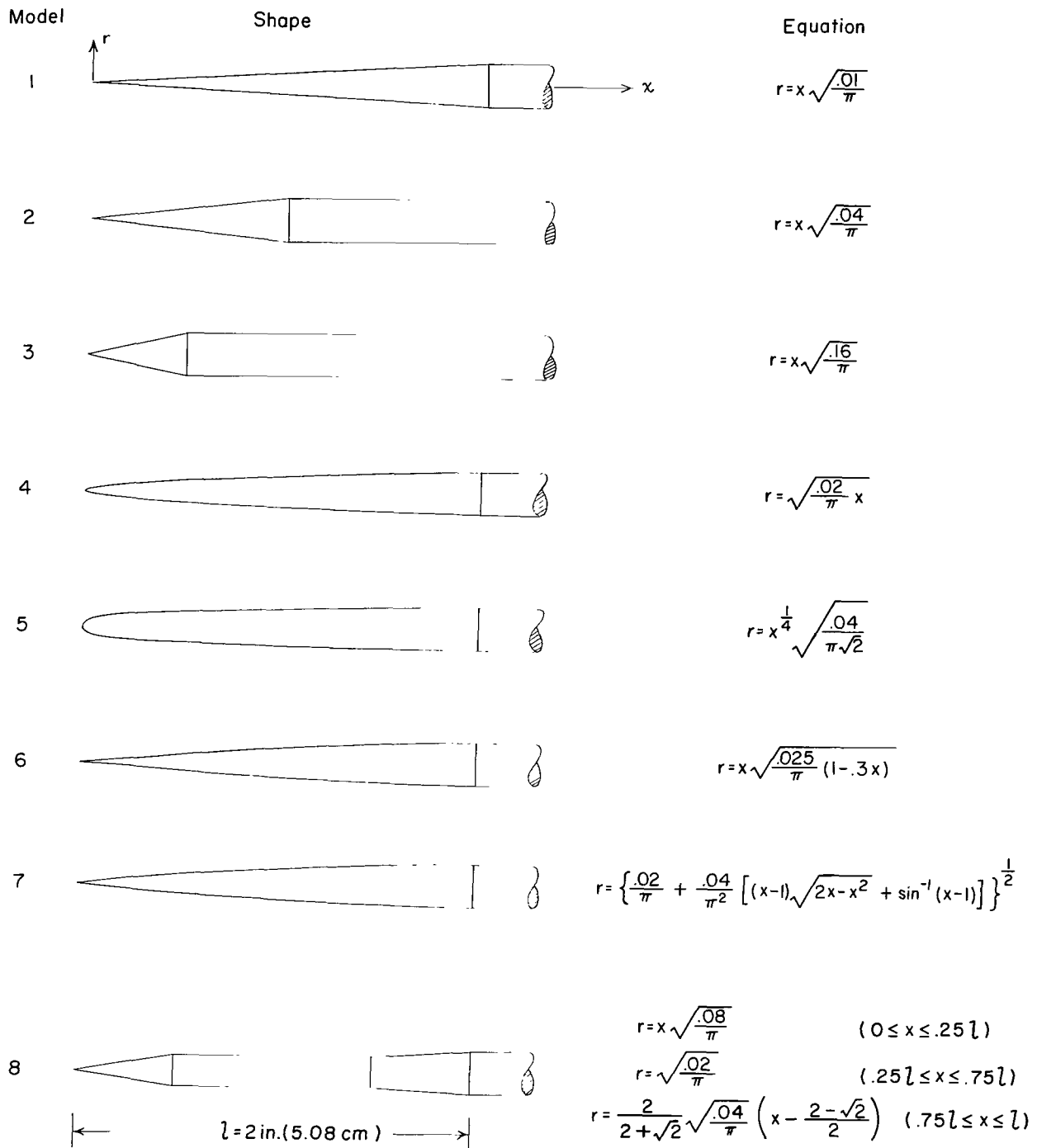


Figure 1.- Sonic-boom test models.

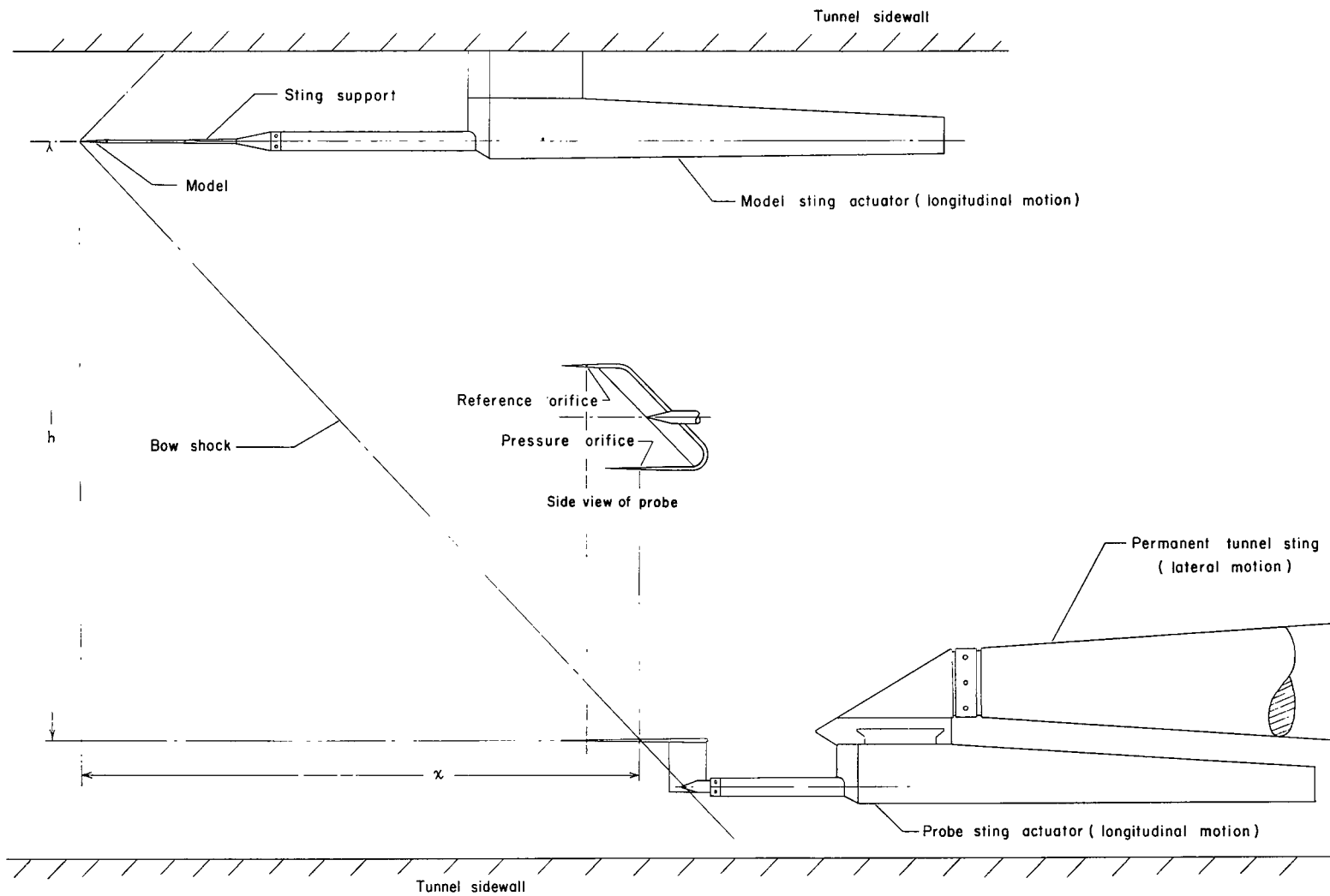


Figure 2.- Wind-tunnel apparatus.

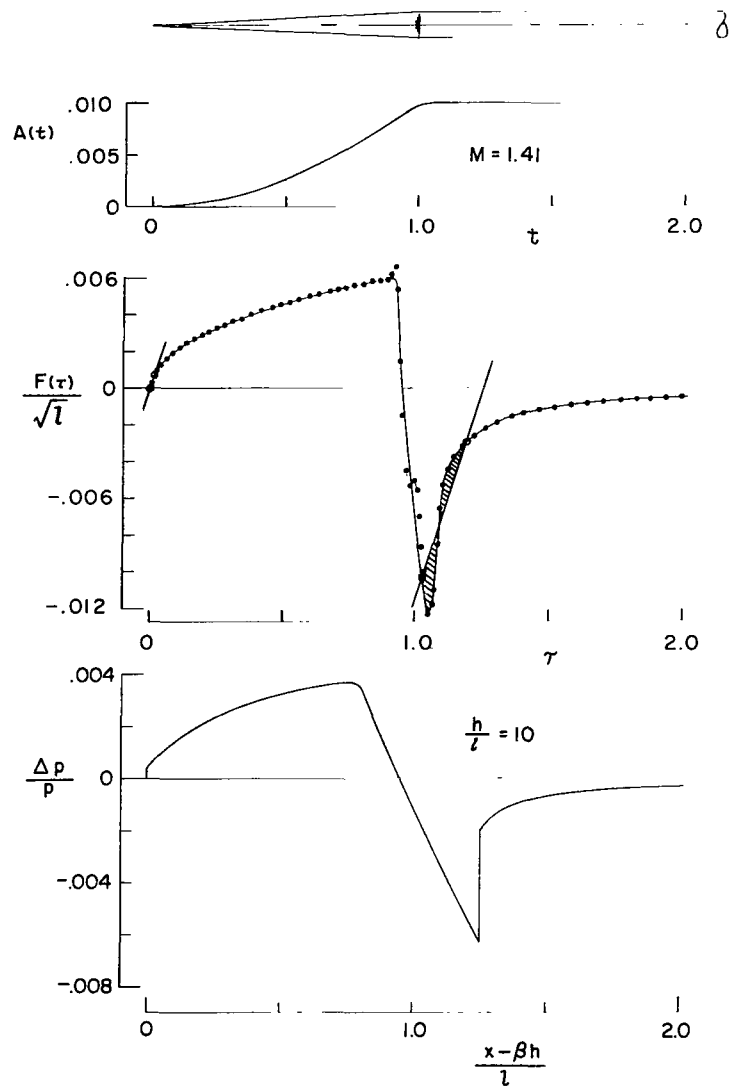
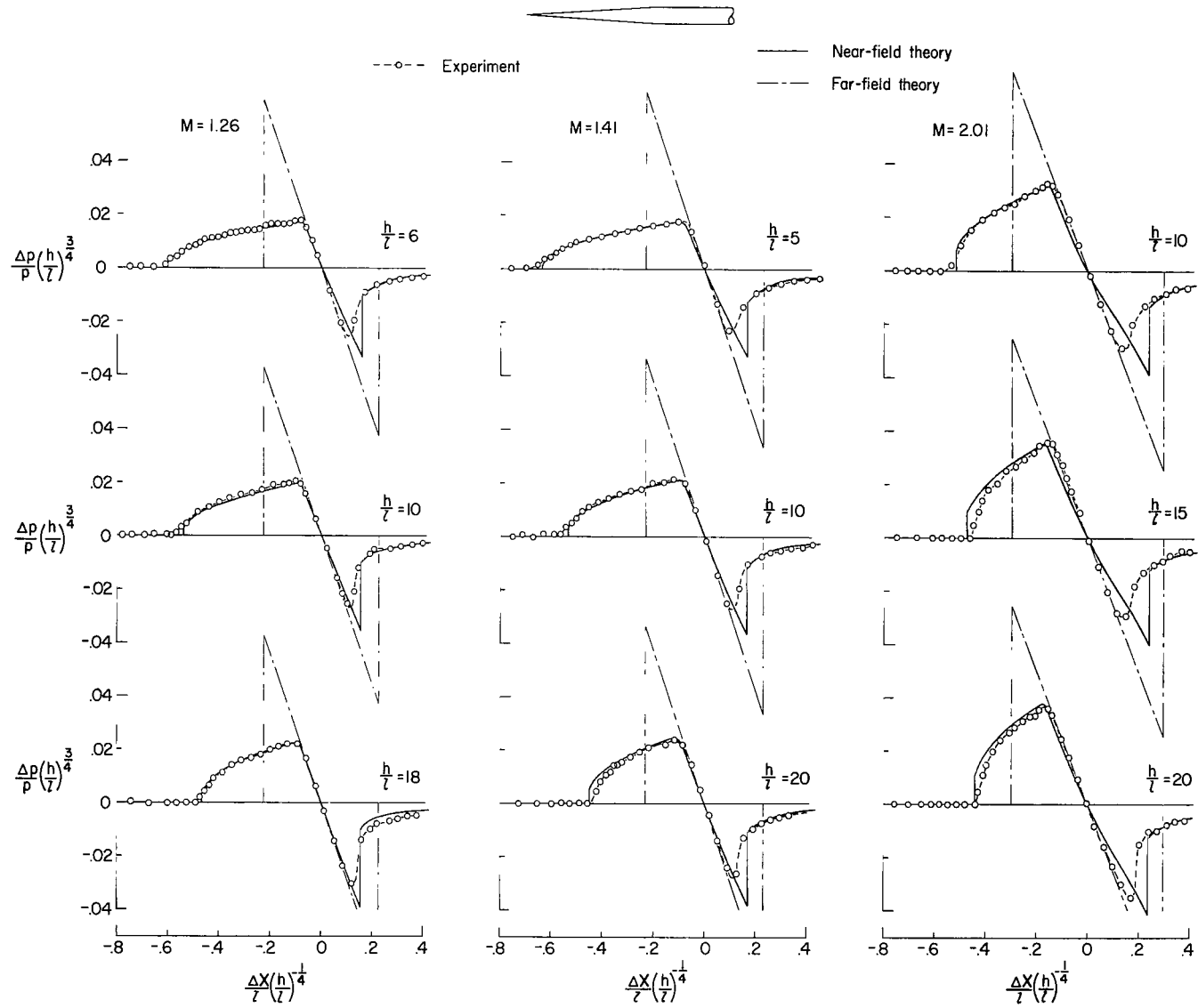


Figure 3.- Method of determining near-field pressure signatures.

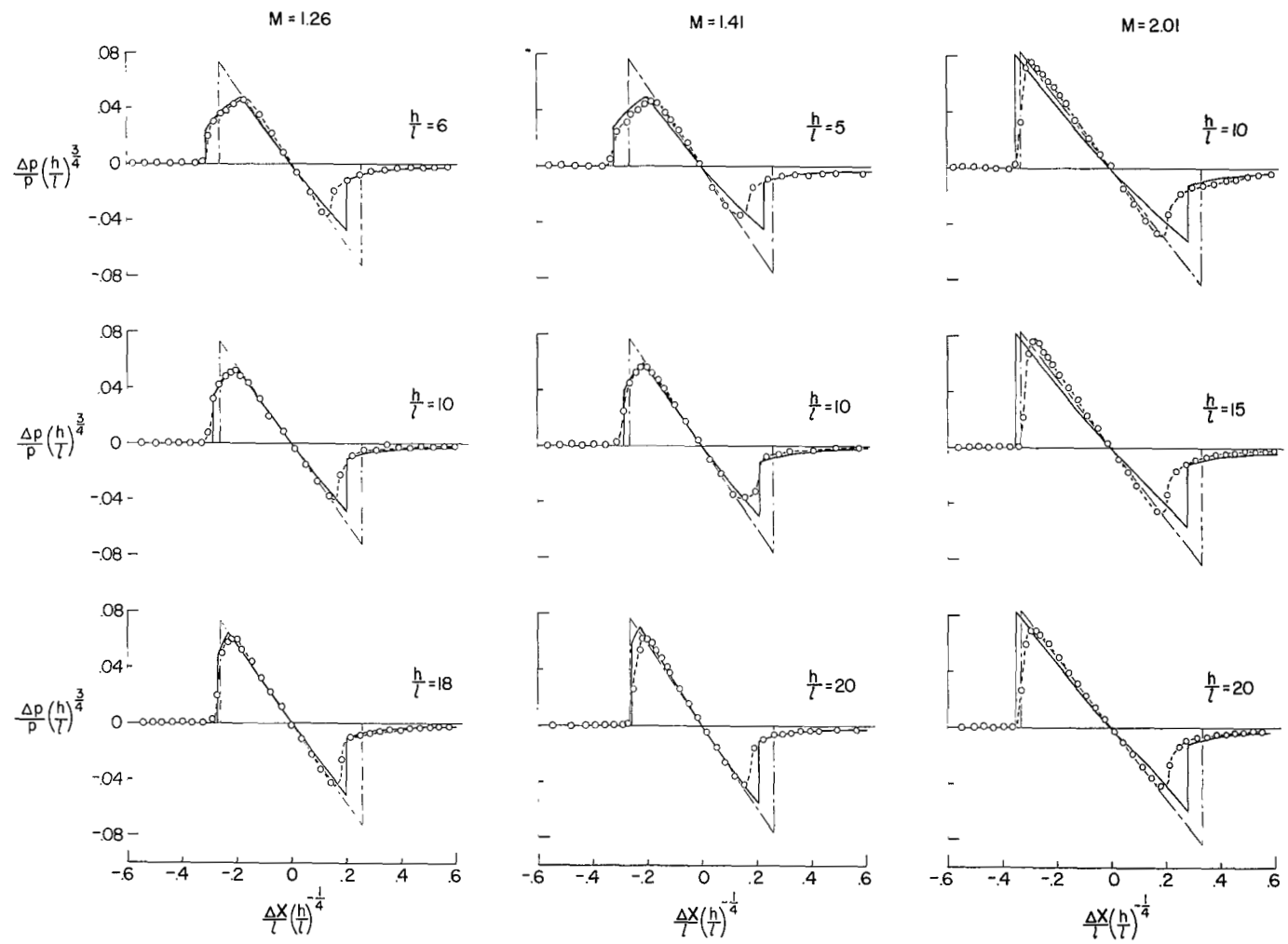


(a) Model 1.

Figure 4.- Pressure distributions in the flow fields of the various models.

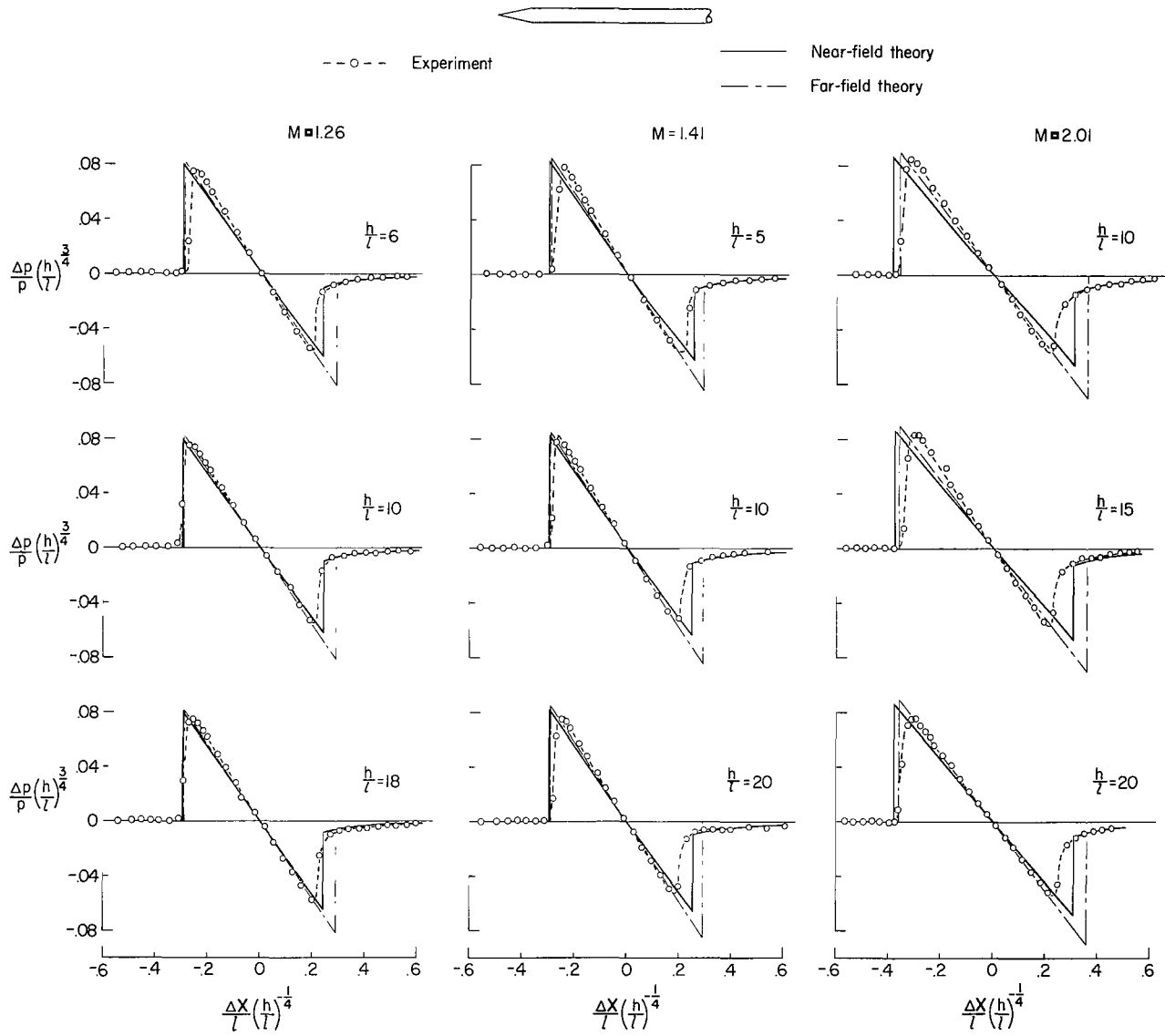


--o-- Experiment ——— Near-field theory
 - - - - Far-field theory



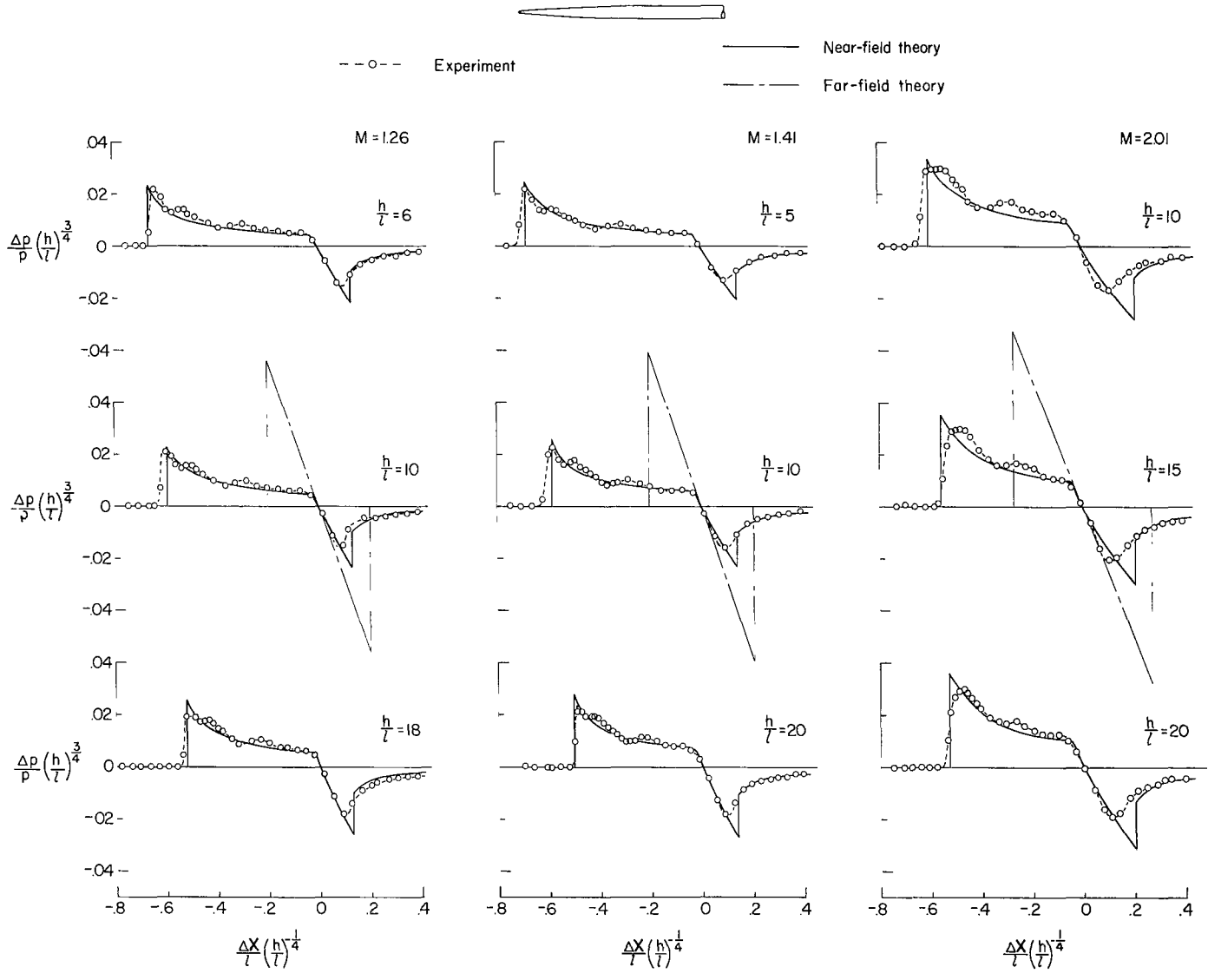
(b) Model 2.

Figure 4.- Continued.



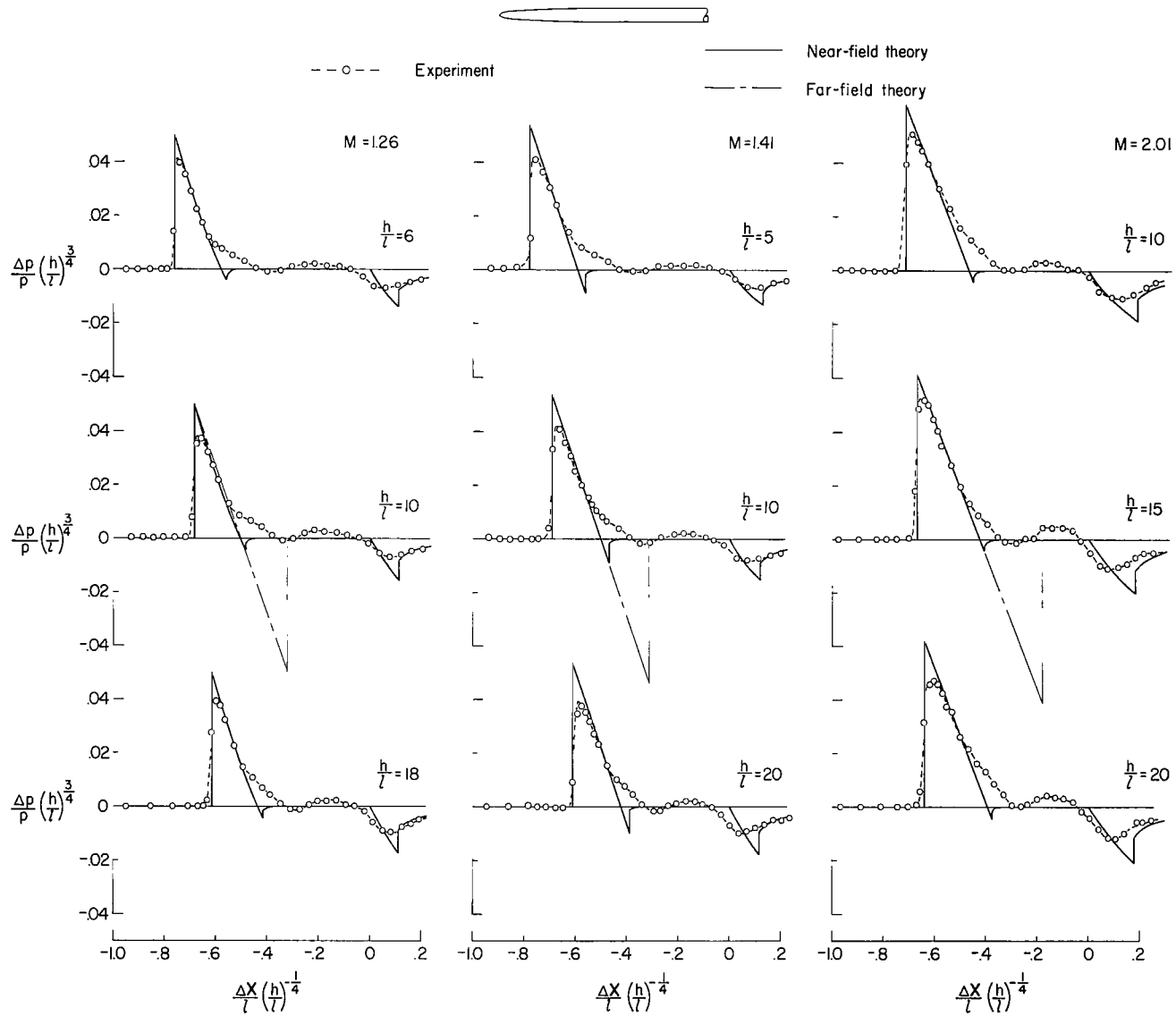
(c) Model 3.

Figure 4.- Continued.



(d) Model 4.

Figure 4.- Continued.



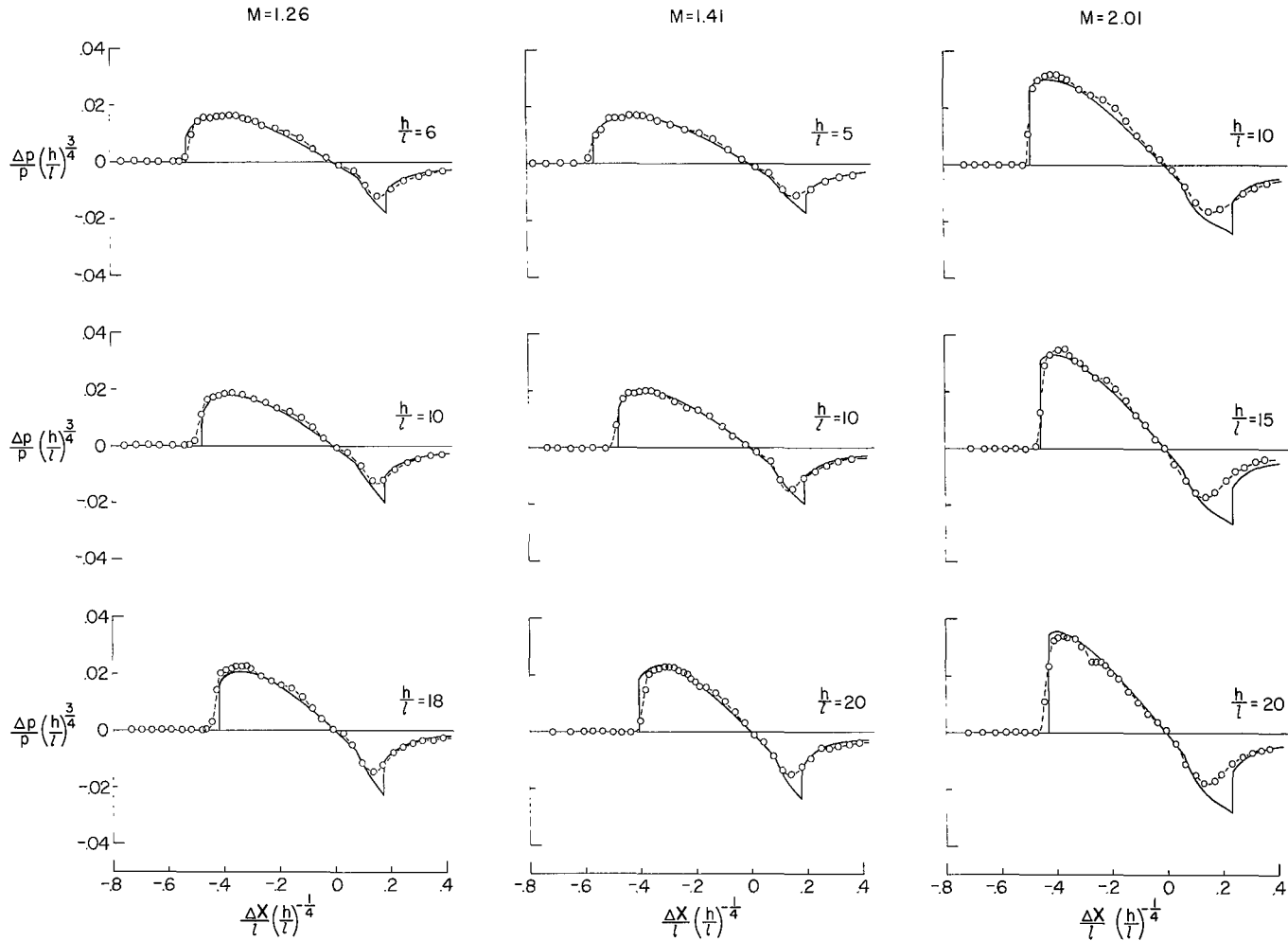
(e) Model 5.

Figure 4.- Continued.



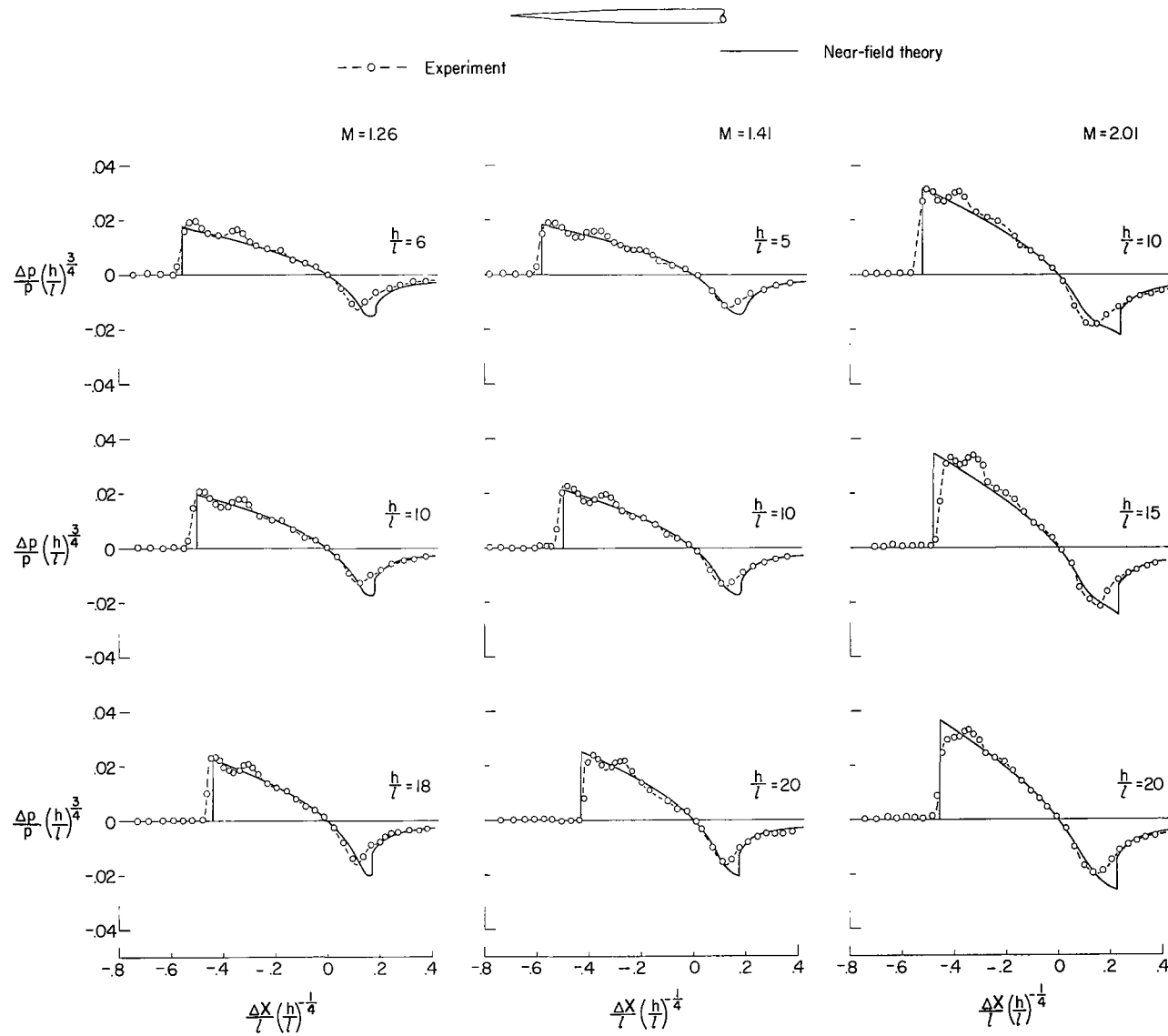
--- Experiment

— Near-field theory



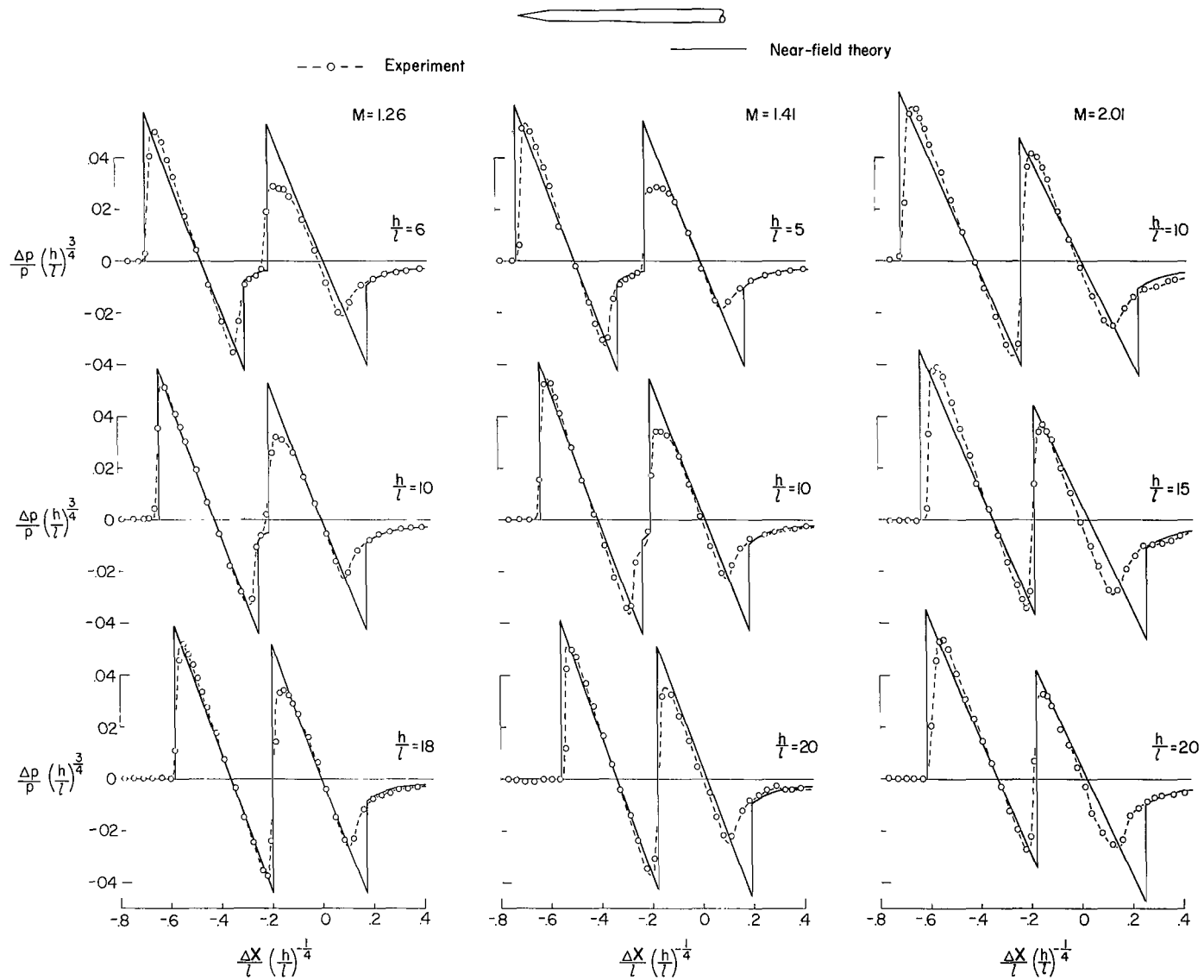
(f) Model 6.

Figure 4.- Continued.



(g) Model 7.

Figure 4.- Continued.



(h) Model 8.

Figure 4.- Concluded.

Model	θ , deg	l_c/l
1	3.24	1.00
2	6.46	.50
3	12.75	.25

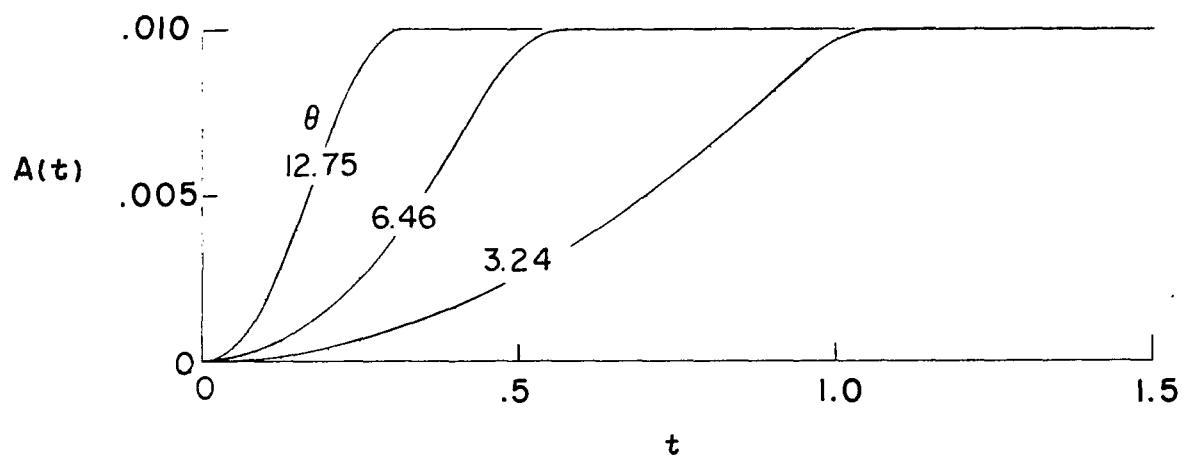
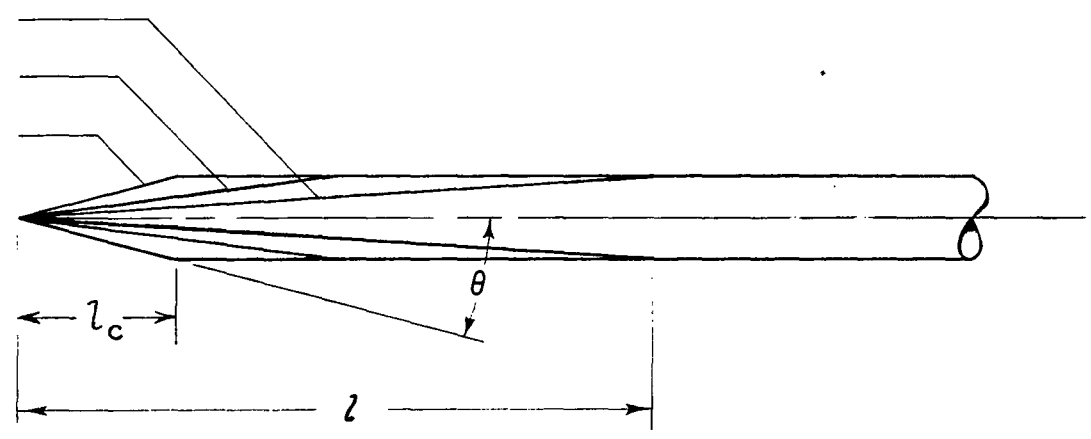


Figure 5.- Models in cone series. $M = 1.41$.

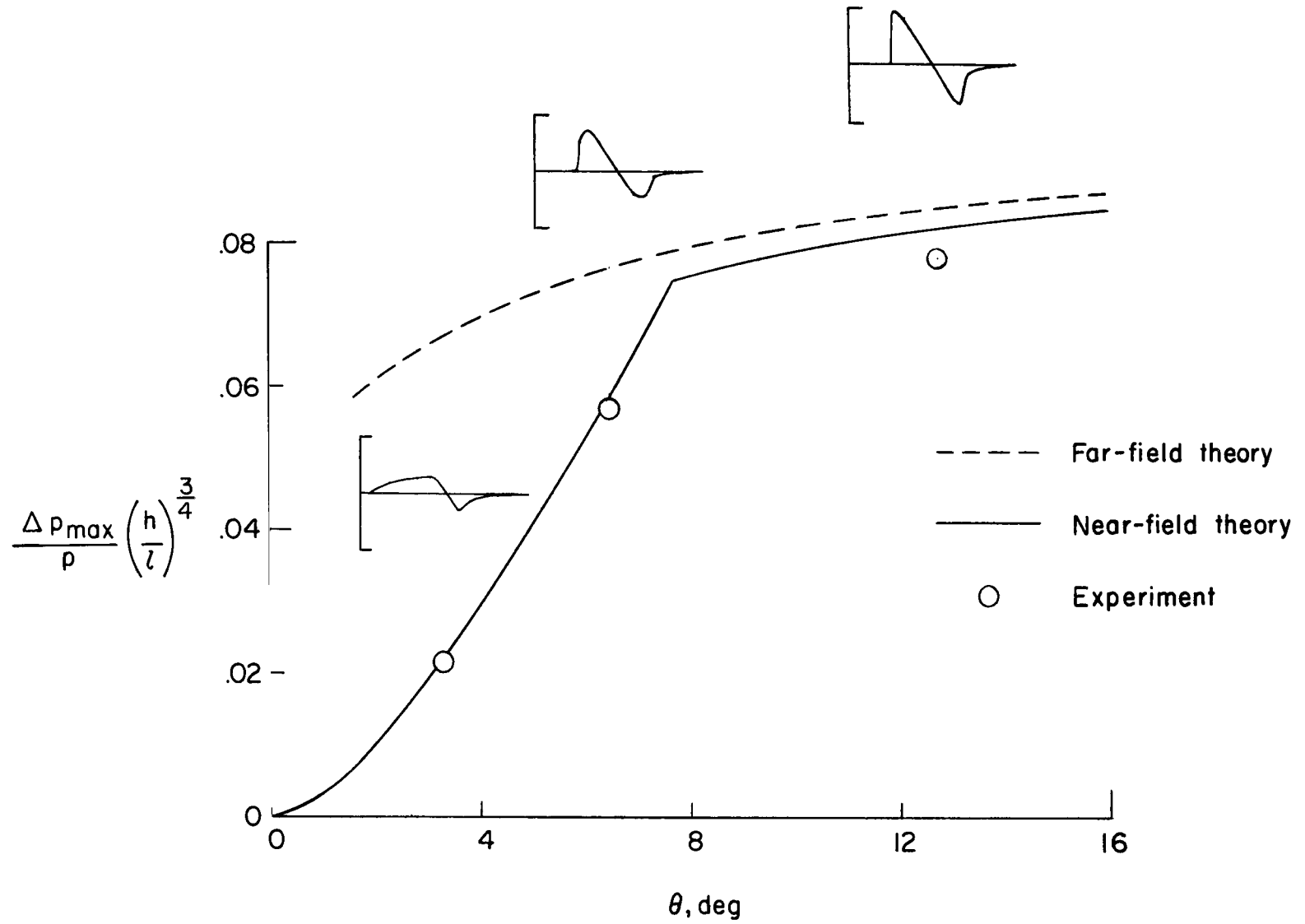


Figure 6.- Variation of maximum-overpressure parameter with cone half-angle. $M = 1.41$; $h/l = 10$.

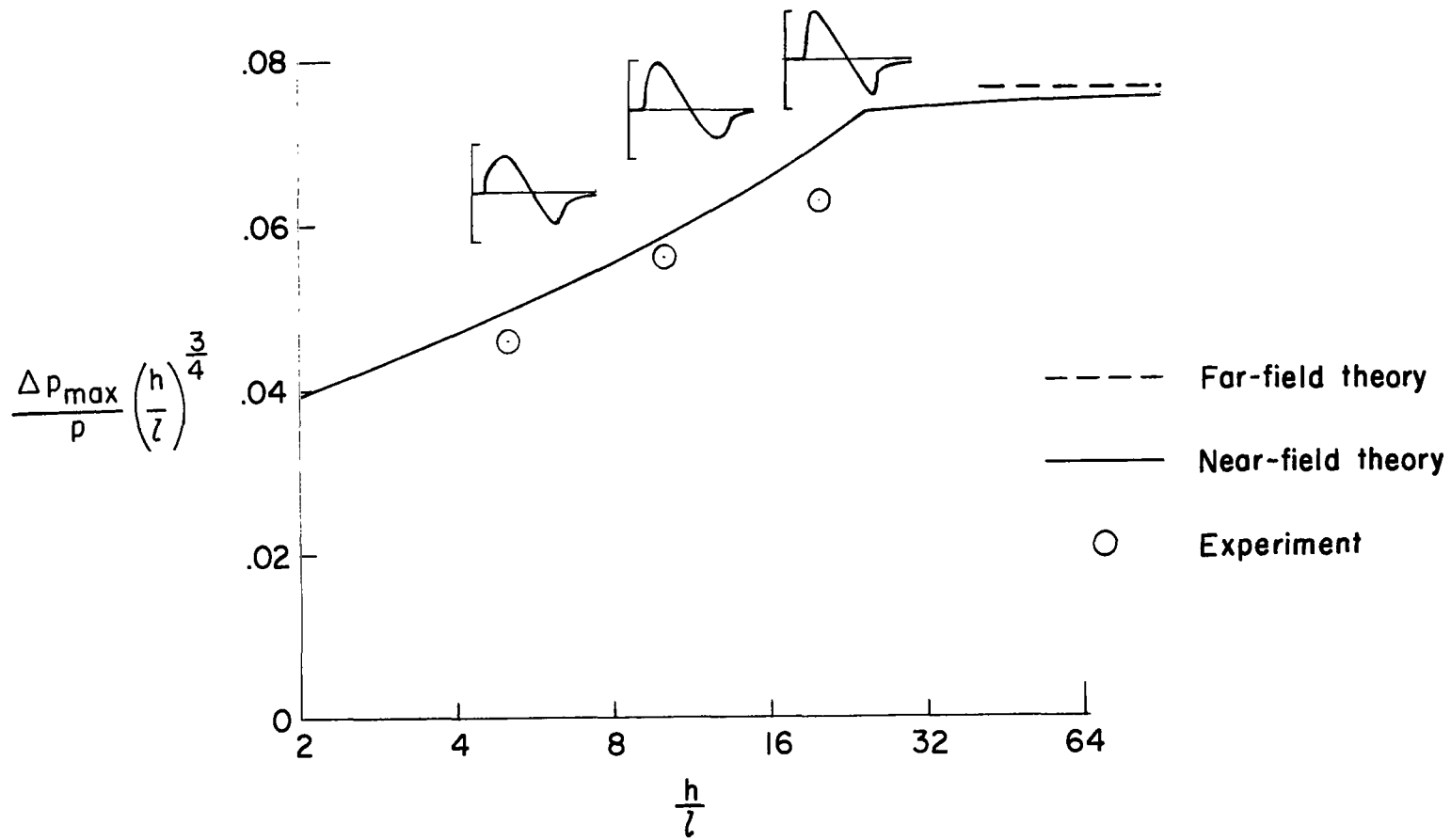


Figure 7.- Variation of maximum-overpressure parameter with distance. Model 2; M = 1.41.

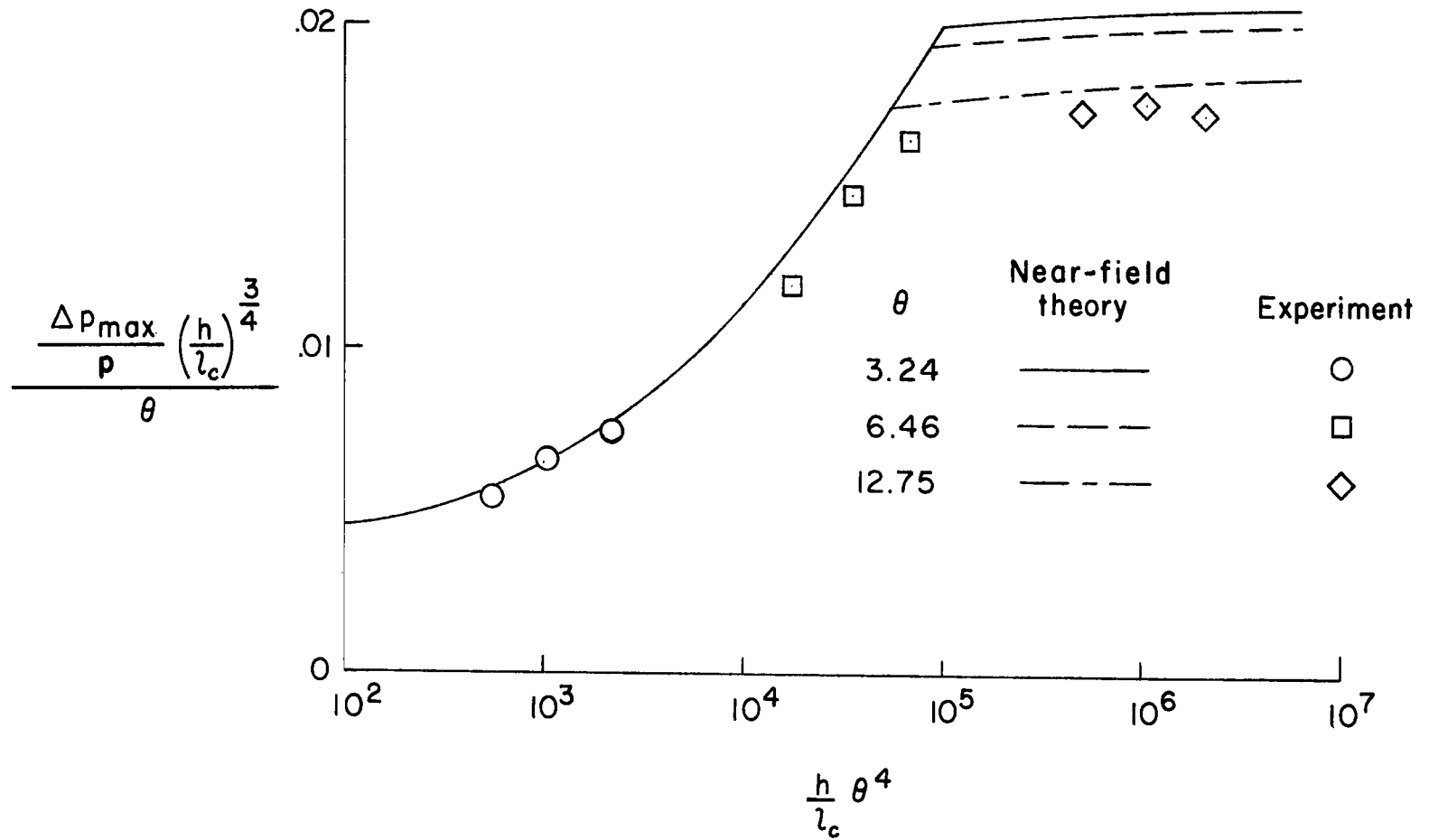


Figure 8.- Variation of maximum-overpressure parameter with cone half-angle and distance. $M = 1.41$.

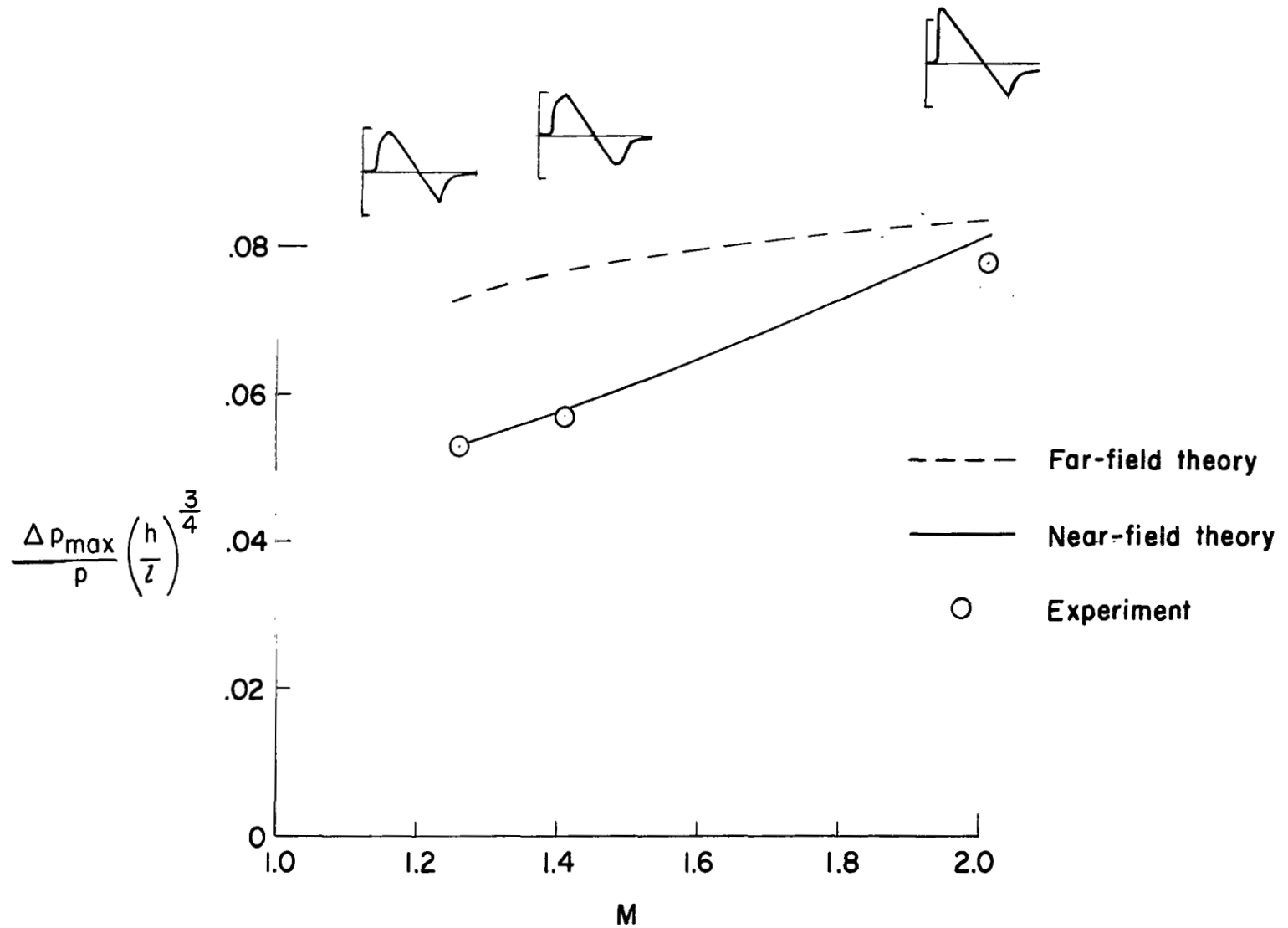


Figure 9.- Variation of maximum-overpressure parameter with Mach number. Model 2; $h/l = 10$.

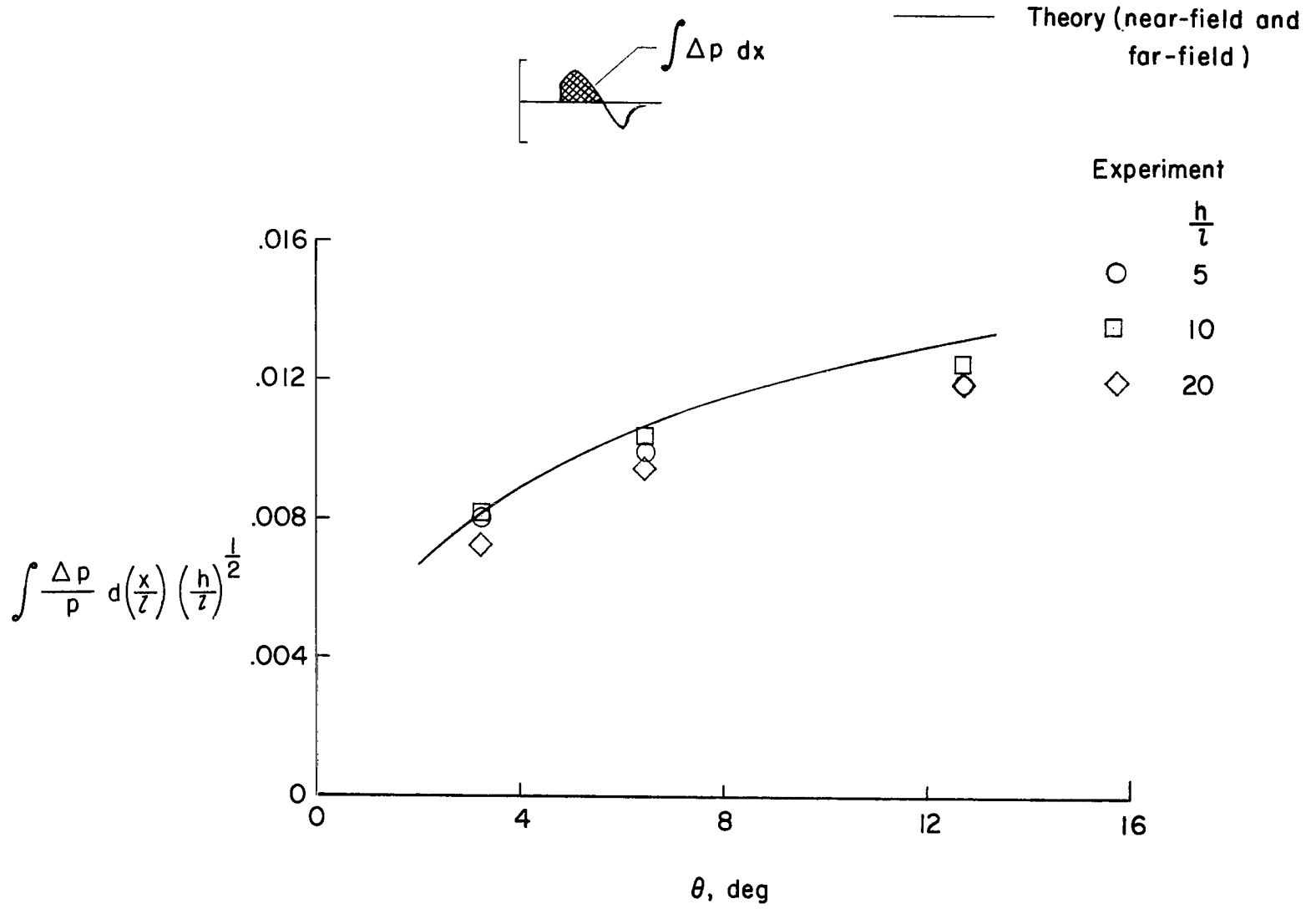


Figure 10.- Variation of signature-impulse parameter with cone half-angle. $M = 1.41$.

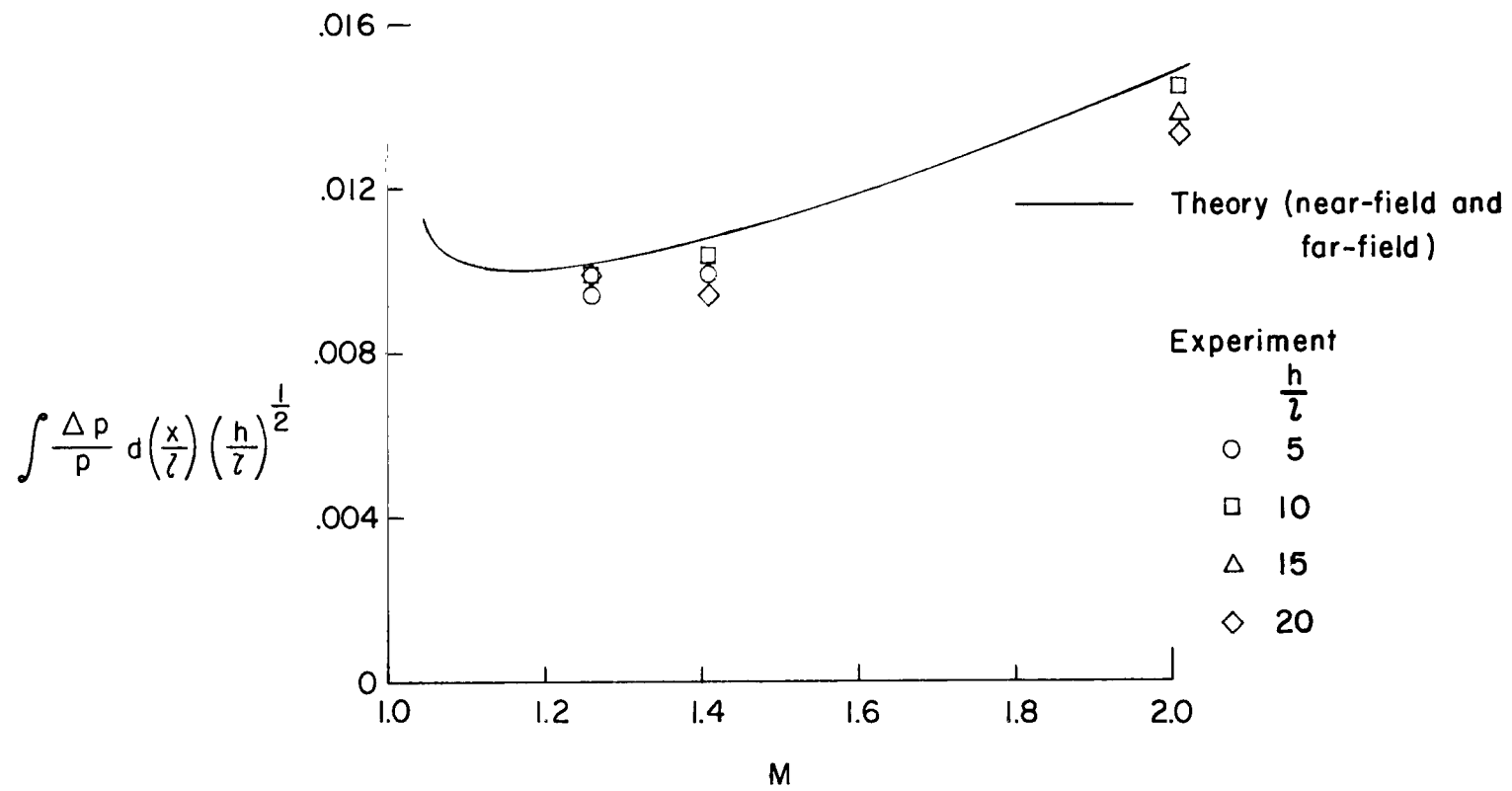


Figure 11.- Variation of signature-impulse parameter with Mach number. Model 2.

Model	n
1	1.00
4	.50
5	.25

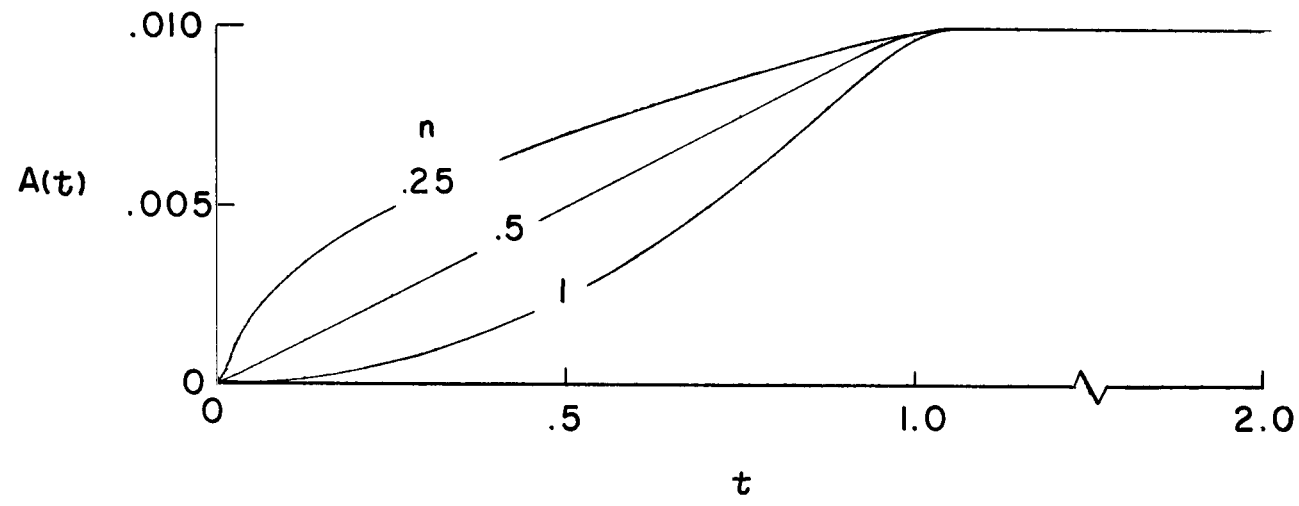
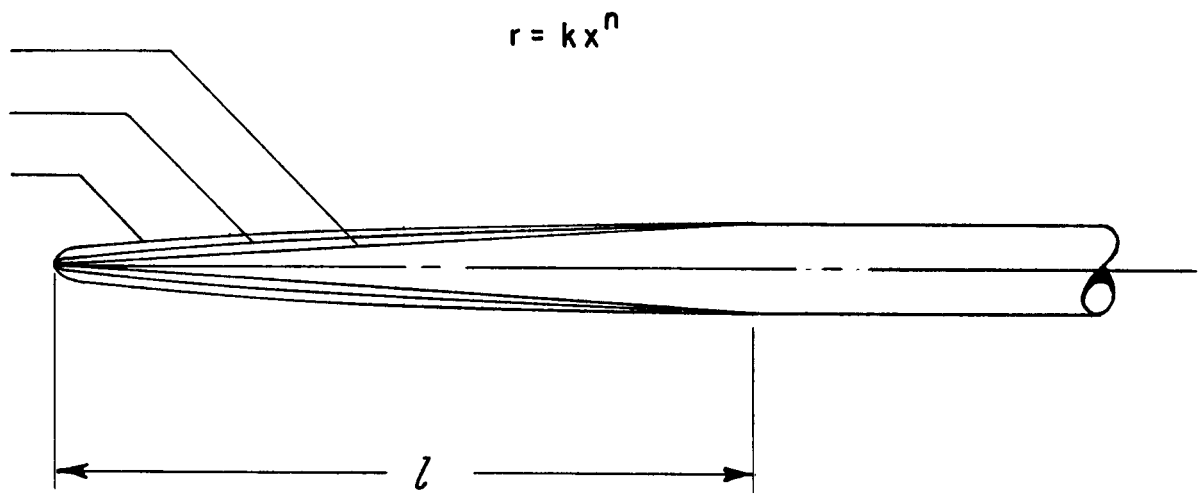


Figure 12.- Models in bluntness series. M = 1.41.

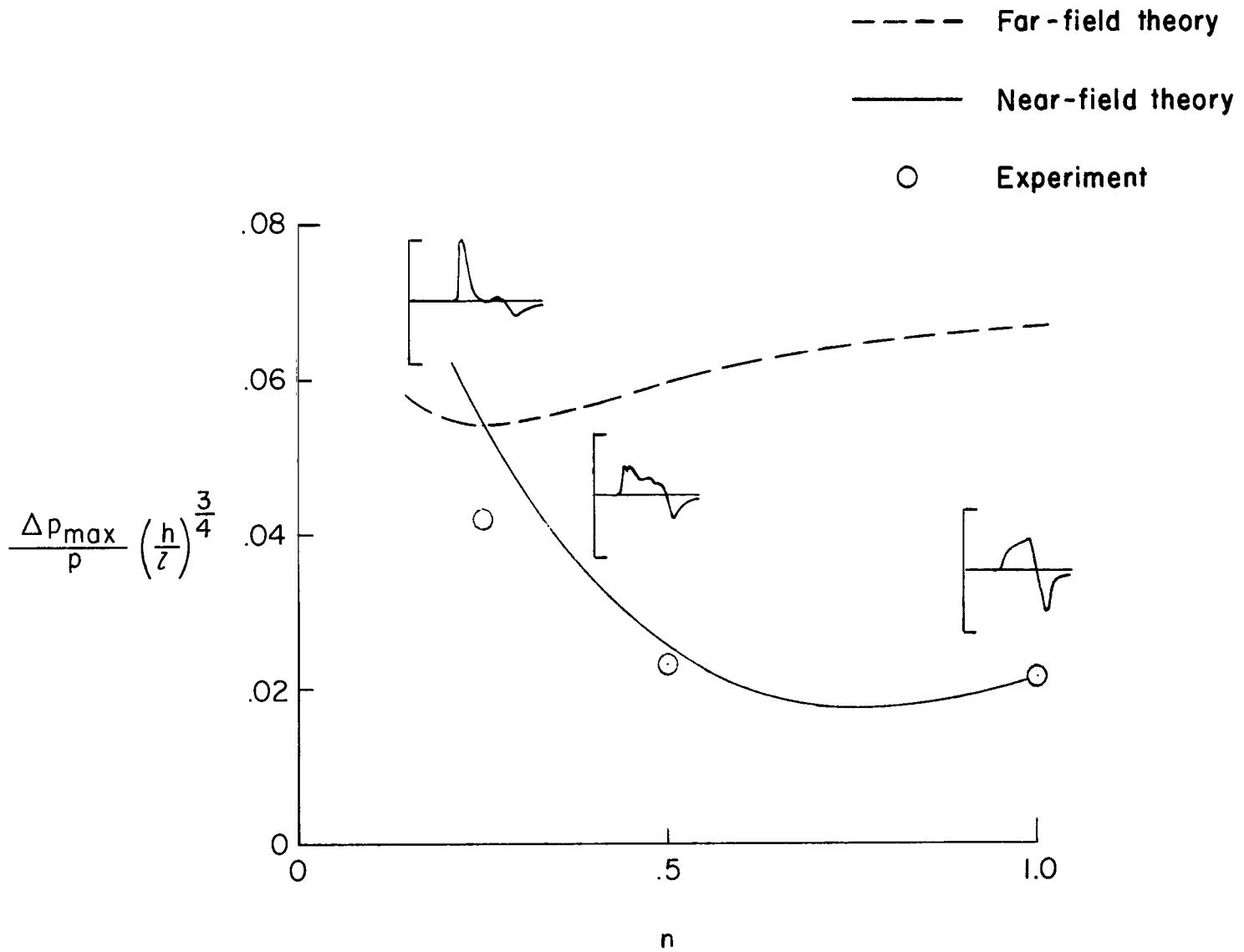


Figure 13.- Variation of maximum-overpressure parameter with bluntness parameter. $M = 1.41$; $h/l = 10$.

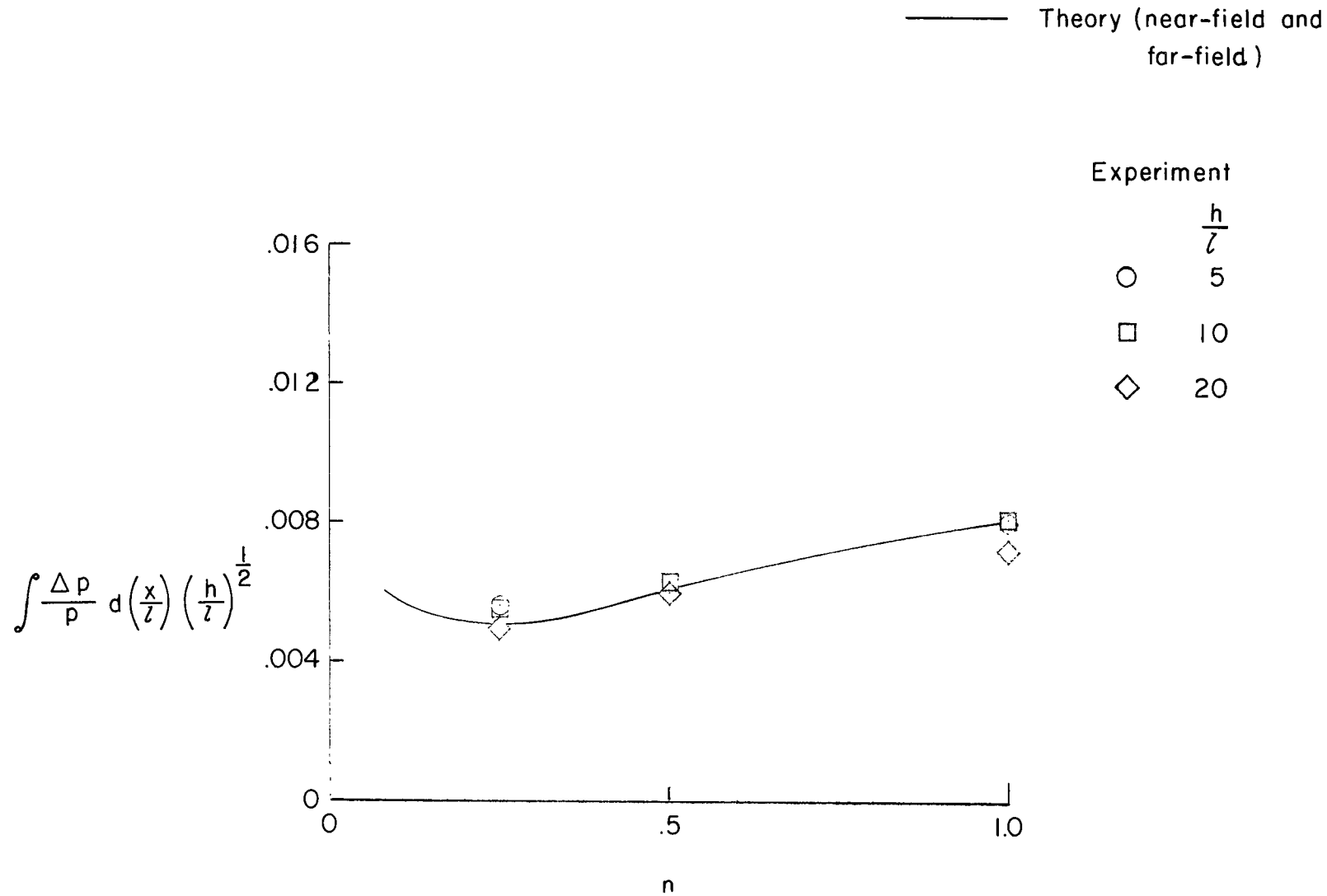


Figure 14.- Variation of signature-impulse parameter with bluntness parameter. $M = 1.41$.

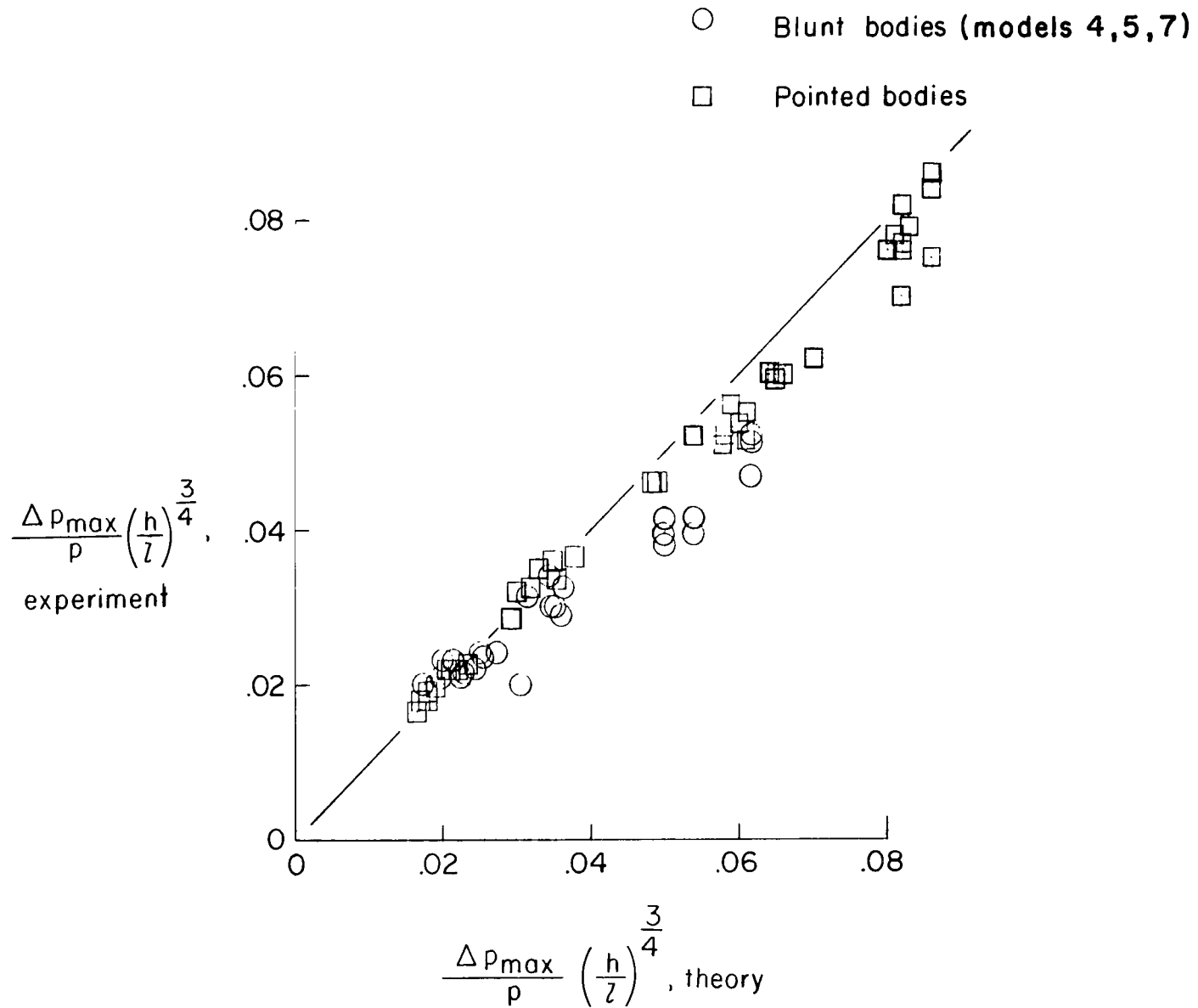


Figure 15.- Correlation of theoretical and experimental overpressure parameters.

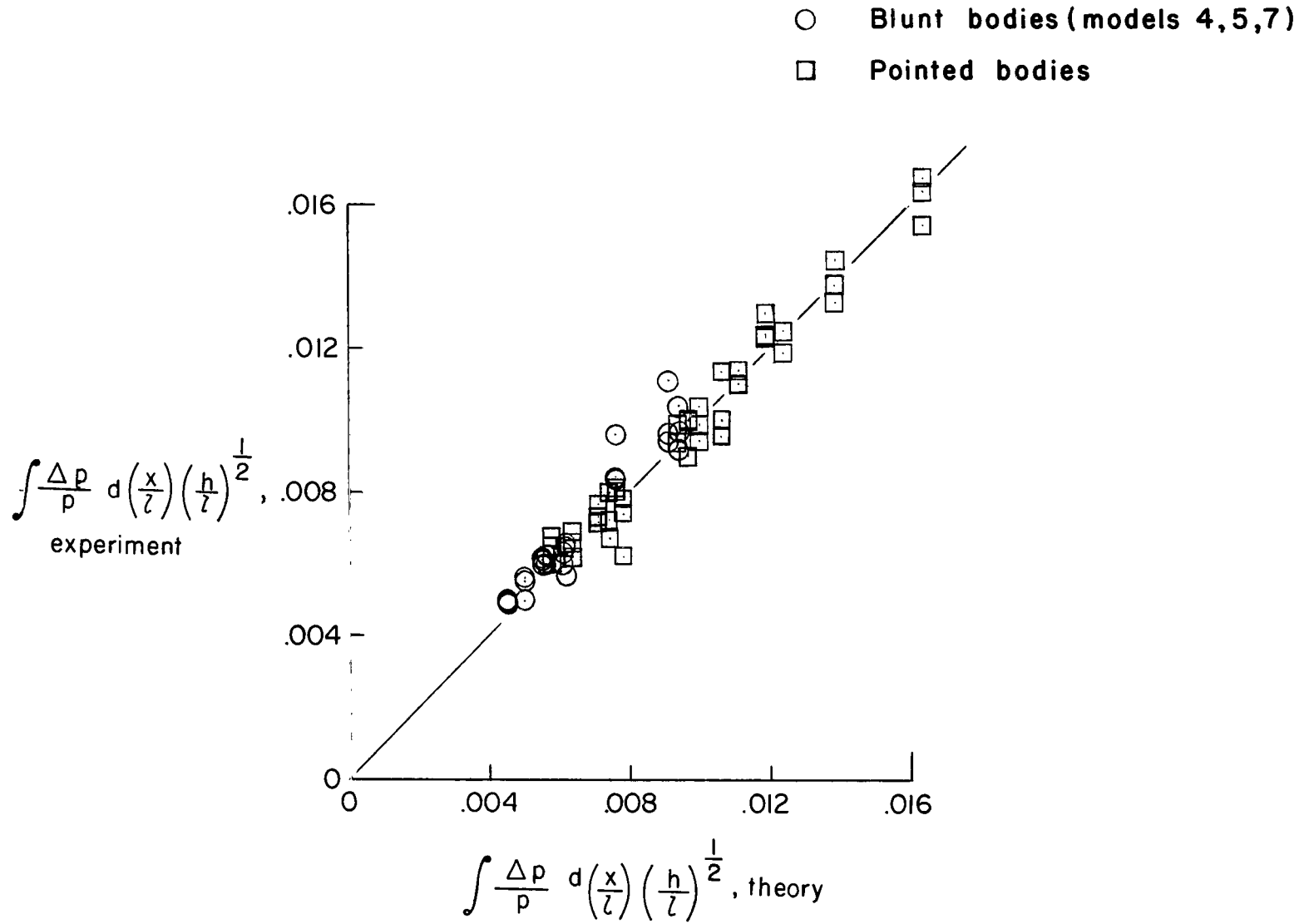


Figure 16.- Correlation of theoretical and experimental signature-impulse parameters.

3/18/75
S

"The aeronautical and space activities of the United States shall be conducted so as to contribute . . . to the expansion of human knowledge of phenomena in the atmosphere and space. The Administration shall provide for the widest practicable and appropriate dissemination of information concerning its activities and the results thereof."

—NATIONAL AERONAUTICS AND SPACE ACT OF 1958

NASA SCIENTIFIC AND TECHNICAL PUBLICATIONS

TECHNICAL REPORTS: Scientific and technical information considered important, complete, and a lasting contribution to existing knowledge.

TECHNICAL NOTES: Information less broad in scope but nevertheless of importance as a contribution to existing knowledge.

TECHNICAL MEMORANDUMS: Information receiving limited distribution because of preliminary data, security classification, or other reasons.

CONTRACTOR REPORTS: Technical information generated in connection with a NASA contract or grant and released under NASA auspices.

TECHNICAL TRANSLATIONS: Information published in a foreign language considered to merit NASA distribution in English.

TECHNICAL REPRINTS: Information derived from NASA activities and initially published in the form of journal articles.

SPECIAL PUBLICATIONS: Information derived from or of value to NASA activities but not necessarily reporting the results of individual NASA-programmed scientific efforts. Publications include conference proceedings, monographs, data compilations, handbooks, sourcebooks, and special bibliographies.

Details on the availability of these publications may be obtained from:

SCIENTIFIC AND TECHNICAL INFORMATION DIVISION
NATIONAL AERONAUTICS AND SPACE ADMINISTRATION
Washington, D.C. 20546